RSC Advances

PAPER

View Article Online
View Journal | View Issue

Cite this: *RSC Adv.*, 2019, **9**, 38183

Structural and magnetization crossover in electrodeposited $FeAl_2O_4$ – effect of *in situ* oxidation

Fazeelat Mukhtar,[ab] Saira Riaz,*[a] Attia Awan,[a] Fatima Rubab,[a] Zohra N. Kayani[b] and Shahzad Naseem[a]

Received 13th June 2019
Accepted 23rd September 2019

DOI: 10.1039/c9ra04455h

rsc.li/rsc-advances

Amongst other spinels, iron aluminium oxide ($FeAl_2O_4$) exhibits exceptional chemical and physical properties. However, magnetic properties of $FeAl_2O_4$ still need further investigation. DC electrodeposition is used to deposit intermetallic Fe_3Al thin films. Oxidation time is varied from 0 to 20 min with a constant metallic layer deposition time of 10 min. Electrodeposited iron aluminium oxide thin films are annealed in the presence of 500 Oe applied magnetic field (MF) at 300 °C in a vacuum. Mixed structural phases, *i.e.* $FeAl_2O_4$ & χ-Al_2O_3, are observed at 5 min, 10 min and 15 min oxidation time. Whereas phase pure $FeAl_2O_4$ is observed at 20 min oxidation time. Magnetization loops show ferromagnetic behavior of iron aluminum oxide thin films with anisotropic nature for in-plane and out-plane configurations. The law of approach to saturation magnetization (LAS) is used to calculate magnetocrystalline anisotropy. Phase purity at 20 min oxidation time results in high saturation magnetization of 29.5 emu cm^{-3} with a low value anistopy constant of 1.28×10^8 erg cm^{-3}. Easy axis of magnetization is shifted from perpendicular to parallel at an oxidation time of 20 min. Results show that *in situ* oxidation of thin films for 20 min leads to structural and magnetization crossover from impure to phase pure $FeAl_2O_4$ thin films with a high value of magnetization.

1. Introduction

Metal oxides have attracted attention from researchers due to various degrees of freedom that coexist in oxides.[1] Magnetic oxides have promising applications in spintronics, *i.e.* memory storage devices,[2,3] because of their possession of high-spin polarization. However, various degrees of freedom in magnetic oxides are not clear because of the presence of oxygen vacancies.[4,5] Therefore, high spin polarization and high Curie temperature (T_c) are some of the basic requirements for a magnetic oxide material to be used in spintronic devices.[6–8]

Iron aluminium oxide possesses a normal spinel structure where A-site cations are filled by Fe^{2+} and B-site cations are occupied by Al^{3+}. However, Fe^{2+} may occupy B-site depending on its synthesis conditions. Intersite exchange of the cations (Fe^{3+} to Fe^{2+} and *vice versa*) and Al^{3+} occurrence are also possible at B-site and tetrahedral sites, respectively.[9–12] The crystal structure of $FeAl_2O_4$ and its structure flexibility, as mentioned above, has been discussed in detail by Harrison *et al.*,[7] Dutta,[8] Fukushima *et al.*[6] and Jastrzebska *et al.*[9] Spinel ferrites depending on degree of inversion possess different types such as (i) normal spinel ferrites (ii) mixed spinel ferrites and (iii) inverse spinel ferrites. Normal spinel structure possesses trivalent cations on octahedral position while divalent cations occupy tetrahedral position. Mixed spinel ferrites have arbitrary arrangement of trivalent & divalent cations on tetrahedral and octahedral sites.[13] Novel physiochemical characteristics of spinel ferrites depend on their chemical composition,[14] microstructure,[15] cation distribution,[16] synthesis methods,[17] annealing, sintering and dopant levels. Transition metal nano ferrites exhibit different saturation magnetizations due to redistribution of cations, and this degree of inversion depends on synthesis method.[18,19]

Scientists used chemical and physical routes including sol–gel,[4,15] thermal evaporation,[16] electrodeposition[17] for the preparation of iron aluminium oxide thin films. To deposit a variety of nanostructures, electrodeposition is very efficient route as described by Low *et al.*,[20] Iselt,[21] Ashby *et al.*[22] and Zhitomirsky *et al.*[23] Electrodeposition is also used to make depositions: (i) for the fabrication of ICs, (ii) for magnetic recording devices and (iii) multilayer structures as reported by Paunovic *et al.*[24]

In the present era, mixed spinel ferrites can be used for the tuning of different properties as discussed by Botta *et al.*[5] and Fukushima *et al.*[6] Fukushima *et al.*[6] prepared iron aluminium oxide ($FeAl_2O_4$) nanoparticles by microwave magnetic field irradiation and conventional heating methods. In conventional heating method the samples were calcined at 1600 °C for 2 min. Single mode cavity system was used for H-field irradiated sample. Ferromagnetic behavior was observed for H-field

[a]Centre of Excellence in Solid State Physics, University of the Punjab, Lahore, Pakistan. E-mail: saira.cssp@pu.edu.pk
[b]Department of Physics, Lahore College for Women University, Lahore, Pakistan

irradiated sample while paramagnetic behavior was observed for conventionally quenched nanoparticles. The magnetization of the sample was larger for magnetic field irradiated than conventional heating method. H-field irradiated sample showed saturation magnetization of 12 emu g^{-1} while conventionally quenched sample showed saturation magnetization of 7.5 emu g^{-1}. Dutta *et al.*[8] used furnace heating method to prepare pure $FeAl_2O_4$ nanoparticles in a nitrogen atmosphere at 450 °C. XRD results confirmed formation of phase pure $FeAl_2O_4$ nanoparticles. Magnetic properties were studied at 300 K & 4 K. Paramagnetic behavior was observed at 300 K while deviation from linear behavior was observed with the decrease of temperature to 4 K and showed some hysteresis. Riaz *et al.*[4] synthesized $FeAl_2O_4$ thin films using an application oriented sol–gel method. The synthesized thin films were annealed at 300 °C in 500 Oe magnetic field. Fe/Al ratio was varied as 0.4, 0.45, 0.5, 0.55 & 0.6. XRD results confirmed formation of phase pure $FeAl_2O_4$ at 0.4 Fe/Al ratio. Whereas, impure phases were observed with the increase of Fe/Al ratio. Strong ferromagnetic behavior was observed for 0.4 ratio while weak ferromagnetic behavior was observed for all other ratios. Yaqoob *et al.*[16] synthesized iron aluminum oxide thin films by thermal evaporation route at 250 °C & 450 °C oxidation temperatures under oxygen flow rate of 10 sccm and observed decrease in saturation magnetization (M_s) values from 0.005 emu to 0.002 emu by increase of oxidation temperature due to presence of impure phases. Imran *et al.*[17] deposited $FeAl_2O_4$ nanostructures by electrodeposition method. They observed that as-deposited nanostructures showed weak ferromagnetic behavior while the magnetic field annealed nanostructures showed strong ferromagnetic behavior. The strong ferromagnetic behavior was observed with the increase of oxidation time. Hafshejani *et al.*[18] used flame spray pyrolysis method for the synthesis and characterization of Fe/Al_2O_3 at 300 K by varying Fe ions in the precursor. In the absence of iron solute two polymorphs of alumina were observed. Whereas, at 0.2 mol.L^{-1} concentration, hercynite $FeAl_2O_4$ was observed.

In the present work, intermetallic Fe_3Al thin films were prepared using electrodeposition method along with magnetic field annealing. Thin films were oxidized for various time intervals, *i.e.* 5–20 min, to obtain iron aluminium oxide thin films; deposition time was kept constant (10 min). As-prepared thin films were subjected to magnetic field annealing (500 Oe externally applied magnetic field) at 300 °C. Structural and magnetic properties have been correlated with the variation in oxidation time.

2. Experimental details

Direct current electrodeposition method was used for the preparation of iron aluminum (Fe_3Al) thin films. The electrolytes were prepared using $Al(NO_3)_3 \cdot 9H_2O$ and $Fe(NO_3)_3 \cdot 9H_2O$. All the reagents, used in the deposition and oxidation were of analytical grade. Boric acid (H_3BO_3), as a buffering agent, was added in the electrolytes. Molarity of the electrolytes were fixed to 0.1 M along with pH of 2. Copper substrates were used to electrodeposit thin films. The role of substrate in the electronics is to provide the interconnections to form an electric circuit and to cool the components of the circuit. Copper is one of the most widely used metals in the world because copper is malleable and ductile. Copper is known by its high thermal and electrical conductivity, and is resistant to corrosion. The melting point of copper is ~1084 °C. Moreover, copper substrate can be easily etched, cleaned and washed before deposition.[19] In this study, the copper substrates were etched using diluted HCl and then ultrasonicated in acetone and isopropyl alcohol for 10 min, separately. Iron aluminum oxide thin films were deposited using three-electrode cell assembly; platinum was used as counter electrode. *In situ* oxidation time was varied in the range 5 min - 20 min by keeping deposition time constant for 10 min. Fig. 1 shows the schematic representation of electrodeposition using three electrode cell assembly.

Electrodeposited iron aluminium oxide thin films were annealed under 500 Oe magnetic field (MF) at 300 °C for 1 hour. X-ray diffractometer (Model: XRD Bruker D8 Advance), was used to study the crystal structure and phase formation. Surface morphology was studied using Carl Zeiss Scanning Electron Microscope (SEM). Room temperature magnetization measurements as a function of magnetic field were studied using Vibrating Sample Magnetometer (Model: VSM Lakeshore's 7407).

3. Results and discussion

3.1. X-ray diffraction

XRD patterns of electrodeposited iron aluminium and iron aluminium oxide thin films MF annealed at 300 °C in vacuum are presented in Fig. 2(a) and in Fig. 2 (b–e), respectively. Oxidation time was varied as 5 min, 10 min, 15 min & 20 min. Intermetallic iron aluminum films showed Fe_3Al structure (JCPDS card #06-0695) with preferred orientation along (220) plane. Whereas, appearance of (311), (400), (422), (440), (620) and (533) planes, after *in situ* oxidation of thin films, confirmed the formation of crystalline spinel structure of iron aluminium oxide ($FeAl_2O_4$) (JCPDS card # 3-0894). Less intense planes (321) & (533) corresponding to χ-Al_2O_3 (JCPDS card # 4-0880) were observed at 5 min, 10 min & 15 min oxidation time. By increase of oxidation time to 20 min chemical phase shift was observed. Such chemical shift resulted in structural crossover from impure to phase pure $FeAl_2O_4$ along with change in preferred orientation from (311) to (400) plane. XRD results have shown that oxidation time played vibrant role for achieving phase pure $FeAl_2O_4$ thin film. Variation in oxidation time resulted in variation in the occupancy of surface energy at tetrahedral site for compensating charges that resulted from oxidation of intermetallic Fe_3Al.[9] At lower oxidation time, *i.e.* 5–15 min, iron and aluminium lattices did not have enough time to activate the stoichiometric ratio of surface ions thus, leading to formation of mixed phases. While at 20 min oxidation time lattices of Fe^{2+} and Al^{3+} had sufficient time for activation of surface ions to produce phase pure spinel $FeAl_2O_4$.[3]

Fig. 2 shows that increase in oxidation time resulted in peak broadening, shifting of the scattering angle (2 theta) and variations in the peak intensity. All these parameters resulted in the

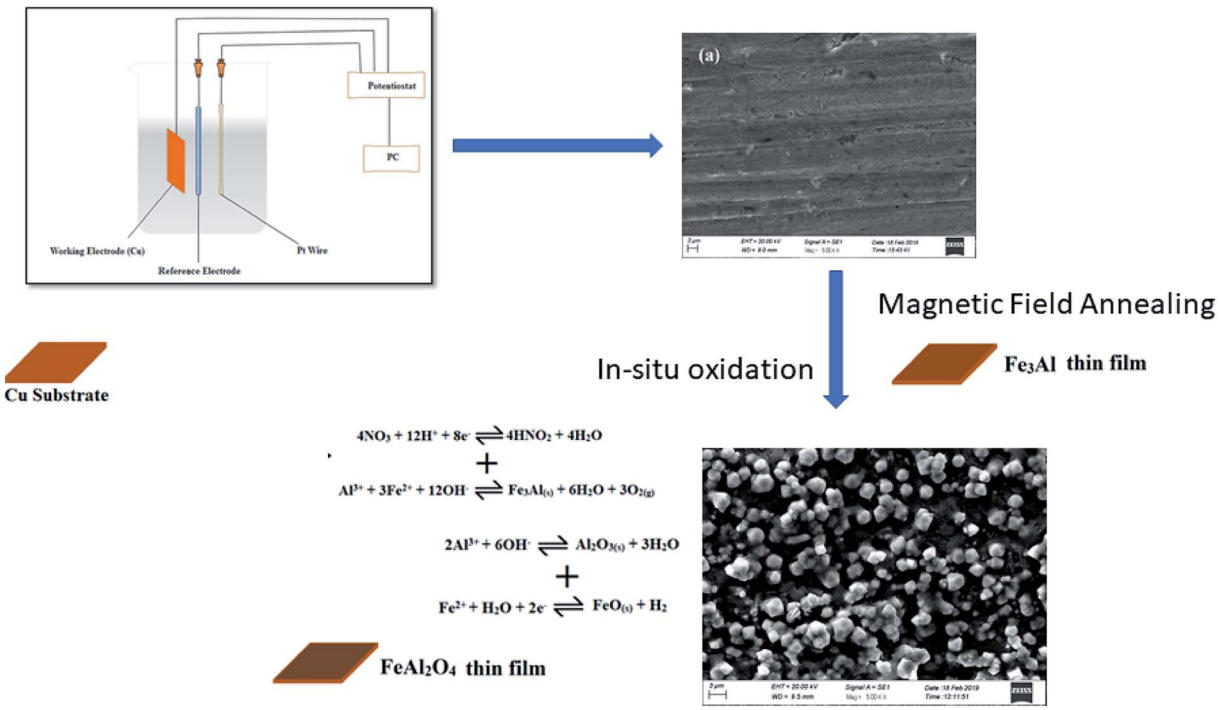

Fig. 1 Schematic representation of electrodeposition of iron aluminium oxide thin films.

variation in crystallite size of thin films. Crystallite size and dislocation density of electrodeposited iron aluminium & iron aluminium oxide thin film were calculated using eqn (1) and (2), respectively.[25]

$$D = \frac{k\lambda}{B\cos\theta} \quad (1)$$

$$\text{Dislocation density} = \frac{1}{D^2} \quad (2)$$

where $k = 0.9$ stands for correction factor, B is full width at half maximum of most intense diffraction peak, λ is wavelength of X-rays and θ stands for Bragg angle.

The crystallite size of Fe_3Al thin film was observed to be ~36 nm. Minimum value of crystallite size was observed for 5 min oxidation time *i.e.* 45.22 nm due to mixed phases *i.e.* $FeAl_2O_4$ & χ-Al_2O_3. Increase in crystallite size along with low value of dislocation density (~3.95×10^{15} lines per m^2) was observed with the increase of oxidation time to 20 min due to appearance of phase pure iron aluminium oxide ($FeAl_2O_4$) crystal structure [Fig. 3(a)]. Higher values of dislocation density were observed for lower oxidation times due to the presence of mixed phases [Fig. 3(b)] as observed in XRD results [Fig. 2]. Thin film development/formation basically depends on two steps (i) nucleation and (ii) growth. Shojaeenezhad *et al.*[26] reported that degree of oxidation increases with increase in oxidation time. Therefore, at higher oxidation time, lattices of iron and aluminum have enough time to react and make new bonds in the presence of oxygen. Further, increased ion concentration beyond certain limit leads to a nucleation process resulting in the elimination of secondary phases as was observed in XRD results.[27–29] Such nucleation process leads to increased value of crystallite size at 20 min oxidation time.[4]

The lattice constant (a), oxygen positional parameter (u), hopping lengths (L_A and L_B), tetrahedral site radius (r_{tetra}) and octahedral site radius (r_{octa}) were calculated by formulae given in eqn (3–9).[4,25]

$$\frac{1}{d_{hkl}^2} = \frac{(h^2 + k^2 + l^2)}{a^2} \quad (3)$$

$$u = \frac{(r_{tetra} + r_O)}{\sqrt{3}a} + \frac{1}{4} \quad (4)$$

$$L_A = \sqrt{3}\, a[\Delta + 1/8] \quad (5)$$

$$L_B = a\sqrt{3\Delta^2 - \frac{\Delta}{2} + \frac{1}{16}} \quad (6)$$

$$r_{tetra} = a\left[u - \frac{1}{4}\right]\sqrt{3} - r_O \quad (7)$$

$$r_{octa} = a\left[\frac{5}{8} - u\right] - r_O \quad (8)$$

$$T = \frac{(r_{tetra} + r_O)}{\sqrt{3}\,(r_{octa} + r_O)} + \frac{(r_O)}{\sqrt{2}\,(r_{tetra} + r_O)} \quad (9)$$

where, hkl = miller indices, d_{hkl} = interplanar spacing, r_o = ionic radii of oxygen and Δ = oxygen positional parameter.

Variations in lattice constant and oxygen positional parameter are shown in Fig. 4(a). The lattice parameter value for Fe_3Al thin film was found to be 5.823 Å which is in good agreement

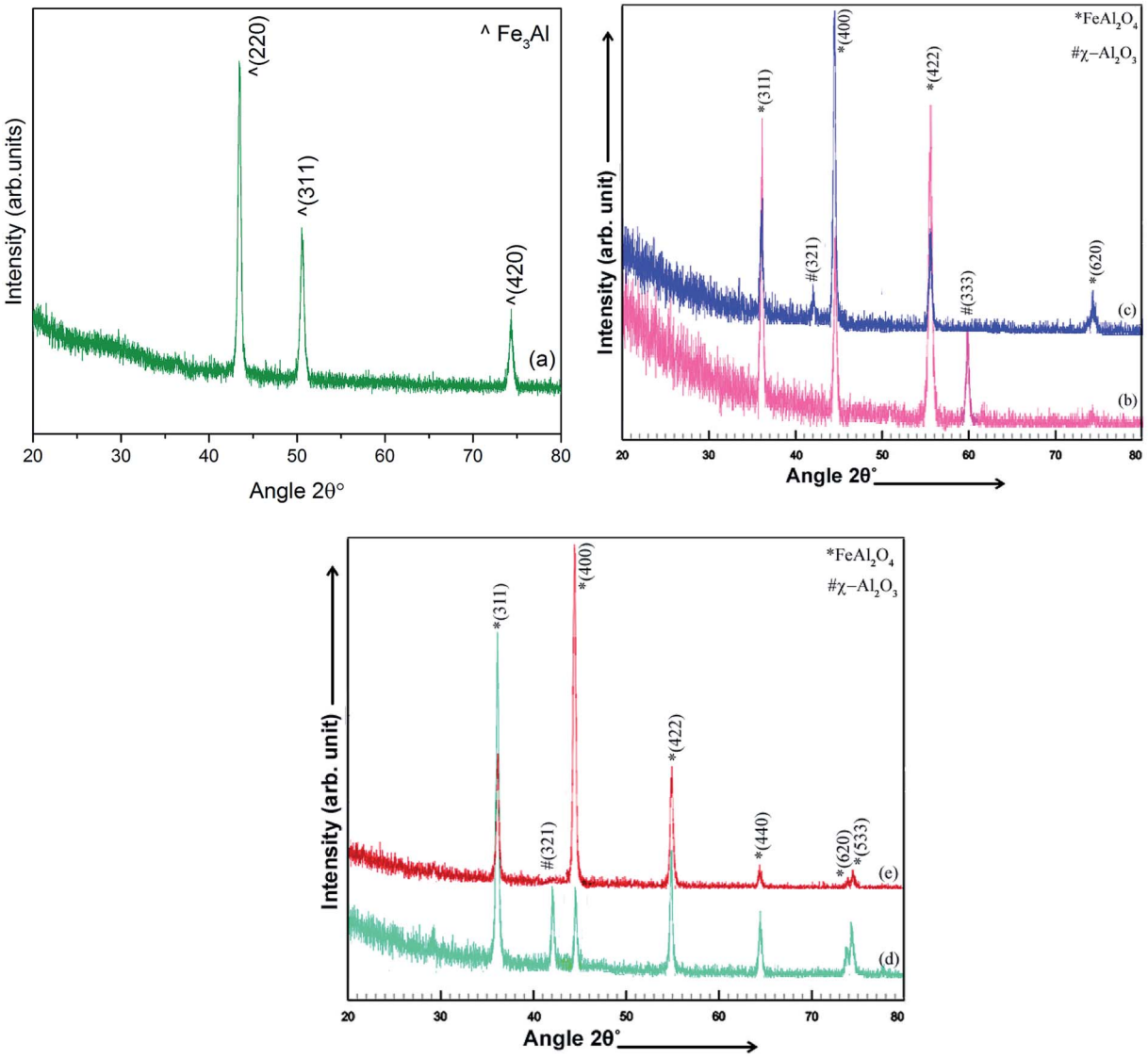

Fig. 2 X-ray diffraction patterns of electrodeposited (a) Fe_3Al and iron aluminum oxide thin films at oxidation time of (b) 5 min (c) 10 min (d) 15 min & (e) 20 min.

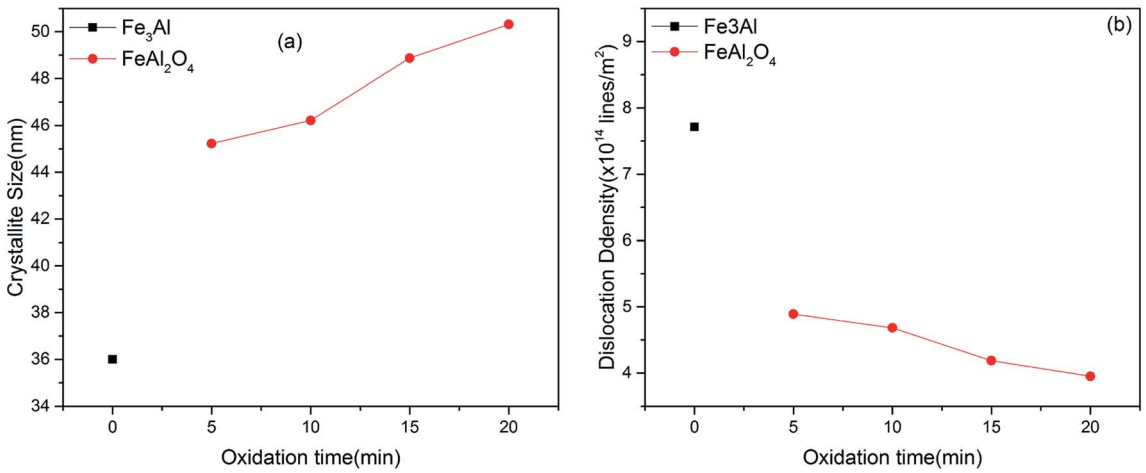

Fig. 3 Variation in (a) crystallite size and (b) dislocation density of iron aluminum & iron aluminium oxide thin film as a function of oxidation time.

with JCPDS card # 06-0695. Increase in lattice parameter from 8.11 Å to 8.14 Å was observed with the increase of oxidation time from 5 to 10 min. Whereas, higher value of lattice parameter was observed for 20 min oxidation time that resulted in the formation of phase pure spinel $FeAl_2O_4$ crystal structure [Fig. 2(e)]. Increase in lattice parameter at 20 min oxidation time has been accredited to increased crystalinity as well as distribution of cations between two possible types of interstitial sites.[30]

Oxygen parameter depends on chemical composition, cation distribution and annealing or sintering conditions.[1] Gabal *et al.*[27] reported that in case of spinel ferrites ideal value for oxygen parameter was 0.375. Fig. 4(a) shows slightly low value of oxygen positional parameter (~0.371) at 20 min oxidation time. Very small variation as compared with the reported value might have been observed due to (a) redistribution of oxygen atoms and (b) reduction of distances between cations and oxygen.[27,31,32]

Variation in hopping lengths and tetrahedral & octahedral radii are given in Fig. 4(b and c). Hopping length 'L_A', the shortest distance of tetrahedral site to oxygen atom, was found to be independent of oxidation time while hopping length 'L_B', shortest distance of octahedral site to oxygen atom, varied with the variation in oxidation time. L_A and tetrahedral radius (r_{tetra}) were found to be 2.01 Å & 75 pm, respectively for $FeAl_2O_4$. L_B and octahedral radius (r_{octa}) was measured to be 1.910 Å and 68.92 pm, respectively for spinel $FeAl_2O_4$.

Several parameters responsible for the variations in structural properties, as a result of *in situ* oxidation include (a) variation in the oxygen content (b) shift in oxygen vacancies' lattice positions, (c) variation in activation energy of cations and (d) transfer of electrons between Fe^{2+} to Fe^{3+} ions.[9,32,33]

According to Williamson–Hall study,[34] microstrain is the source of peak broadening of diffraction line. Williamson–Hall model changes to uniform deformation model when the microstrain is considered to be same in all crystallographic orientations. In the uniform deformation model, mechanical properties of electrodeposited thin films are found to be independent of the crystallographic orientations. According to Hook's law, using uniform deformation stress model, stress has a linear relation with strain, and maximum strain is calculated by the relation given in eqn (10) (ref. 25) and plotted in Fig. 5(a).

$$\frac{\Delta d}{d} = \frac{B}{4\tan\theta} \tag{10}$$

where $\Delta d/d$ is microstrain, B is FWHM of preferred orientation and θ is the diffraction angle.

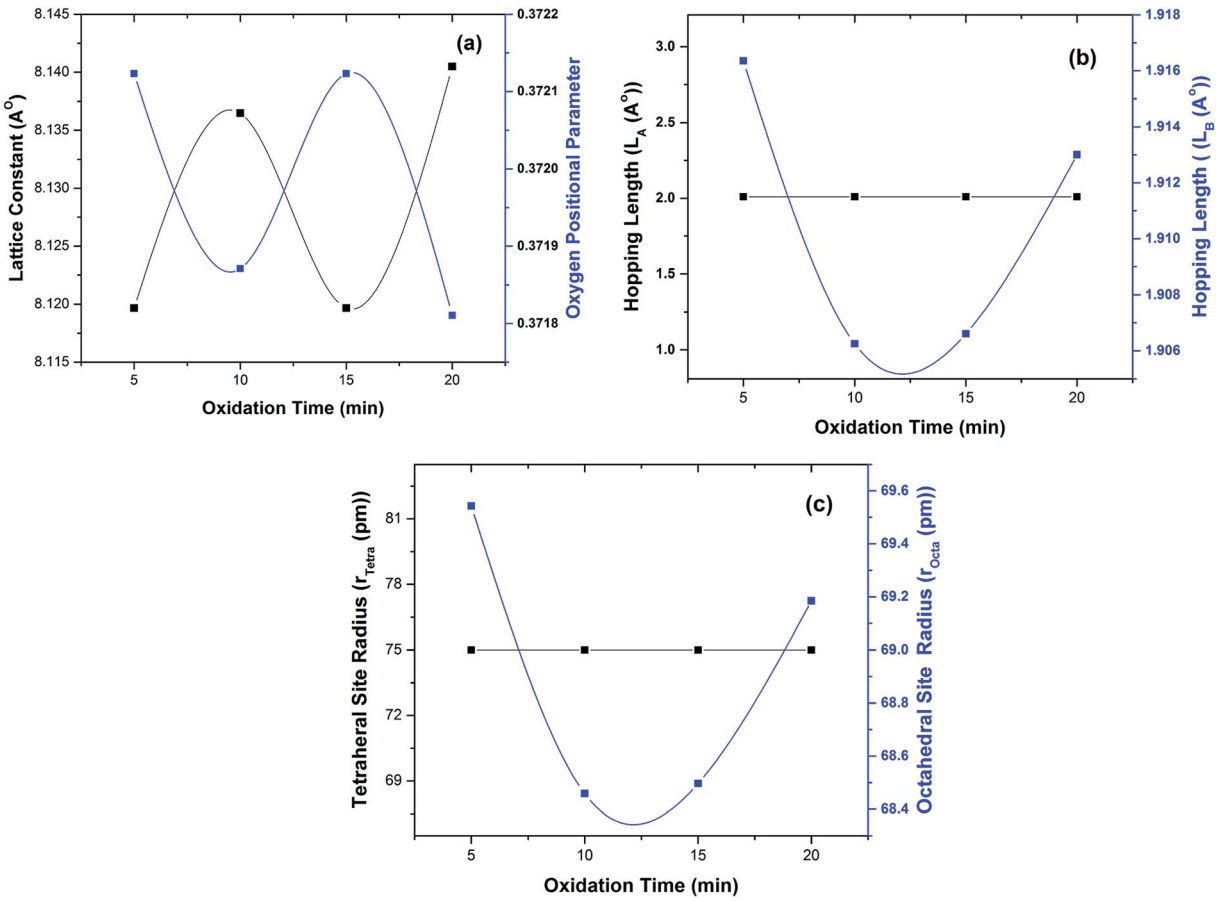

Fig. 4 Variation in (a) lattice constant and oxygen positional parameter, (b) hopping lengths (L_A and L_B) and (c) radii of tetrahedral & octahedral sites.

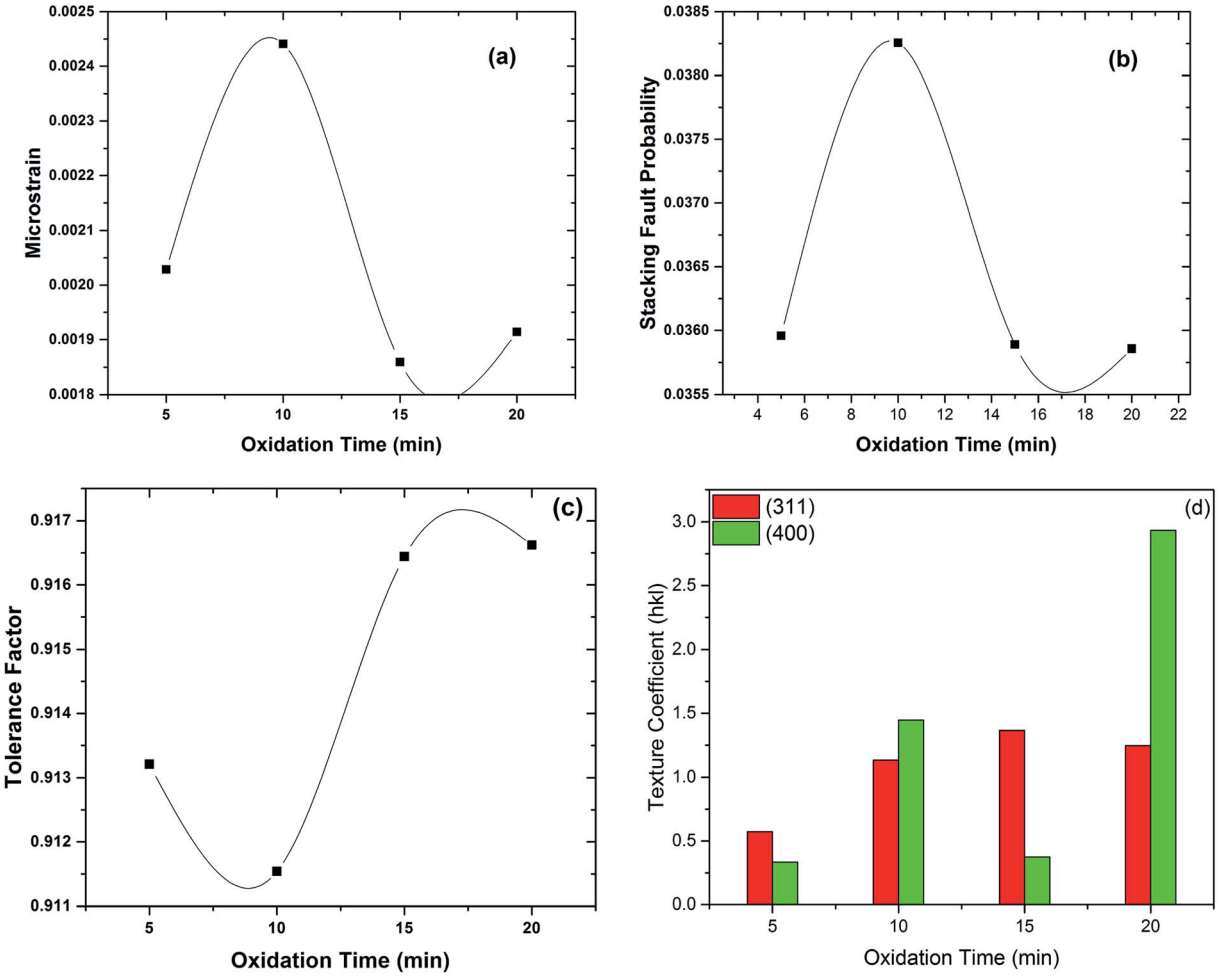

Fig. 5 Variation in (a) microstrain, (b) stacking fault probability, (c) tolerance factor and (d) texture coefficient as a function of oxidation time.

Stacking fault probability is defined as an interruption of the normal stacking sequence of atomic planes in close-packed crystal structure. In the face centered cubic (fcc) crystal structure, the stacking sequence is ABCABCABC. A stacking fault appears when any kind of disturbance takes place in this sequence. Stacking faults are classified as intrinsic and extrinsic faults.[25,33] These faults can directly be corelated to the microstrain induced in thin films. At 5 min & 10 min oxidation time relatively higher value of microstrain and stacking fault probability was observed due to presence of mixed phases [Fig. 5(a) and (b)]. Whereas, lower value of microstrain and stacking fault probability was observed for 20 min oxidation time due to the formation of phase pure iron aluminium oxide spinel ($FeAl_2O_4$) thin film.

Tolerance factor for ideal spinel structure is equal to unity.[9] Slightly lower value of tolerance factor was observed at 5 min, 10 min & 15 min oxidation time because of the presence of χ-Al_2O_3 traces as were observed in XRD patterns [Fig. 2(b–d)]. Tolerance factor for electrodeposited iron aluminium oxide thin film with 20 min oxidation time was close to unity representing the formation of thin film with minimum defects[9] as shown in Fig. 5(c).

Texture coefficient (TC) shows the preferred orientation of thin films that can be calculated by eqn (11) (ref. 25) given below:

$$\mathrm{TC}_{(hkl)} = \frac{\frac{I_{o(hkl)}}{I_{c(hkl)}}}{1/N \sum \frac{I_{o(hkl)}}{I_{c(hkl)}}} \quad (11)$$

where $I_{o(hkl)}$ = observed intensity, $I_{c(hkl)}$ = relative intensity taken from JCPDS card no: 3-0894, N shows the number of diffraction lines.

Transformation among various crystallographic phases (*i.e.* from impure to phase pure) lead to change in preferred crystal orientation. The values of texture coefficient for (311) & (400) planes are shown in Fig. 5(d). It has been observed in XRD patterns that preferred orientation changed from (311) plane to (400) plane with the increase of oxidation time from 15 min to 20 min [Fig. 2(d and e)] resulting in structural crossover from impure to phase pure iron aluminium oxide thin film.

The cation distribution at interstitial sites may be expressed as given below.[31]

Table 1 Cation distribution of $FeAl_2O_4$ System

Deposition time (min)	Oxidation time (min)	Tetrahedral site		Octahedral site	
		Fe^{2+}	Al^{3+}	Fe^{2+}	Al^{3+}
10	5	0.975237	0.024763	0.024763	1.975237
10	10	0.988385	0.011615	0.011615	1.988385
10	15	0.987925	0.012075	0.012075	1.987925
10	20	0.979576	0.020424	0.020424	1.979576

$$Fe_{\delta}\,Al_{1-\delta}\,[Fe_{1-\delta}\,Al_{1+\delta}]O_4$$

Tetra Octa

Eqn (12) and (13) are used to calculate cation radius at tetrahedral and octahedral sites.[25,31]

$$r_{tetra} = \delta r_{Fe} + (1 - \delta) r_{Al} \quad (12)$$

$$r_{octa} = (1 - \delta) r_{Fe} + (1 + \delta) r_{Al} \quad (13)$$

Subtracting eqn (12) from (13) led to:

$$\delta = \frac{(r_{tetra} - r_{octa} + r_{Fe})}{2(r_{Fe} - r_{Al})} \quad (14)$$

δ was calculated by putting values of ionic radius of iron (r_{Fe}), ionic radius of aluminium (r_{Al}), tetrahedral site radius (r_{tetra}) and octahedral site radius (r_{octa}) in eqn (14). The values of cation distribution at tetrahedral and octahedral sites are listed in Table 1 that confirmed the formation of iron aluminum oxide thin film.

The configuration of ion pairs in spinel ferrites with favorable distances and angles for magnetic interactions are shown in Fig. 6. The interionic distances (*i.e.* values of edge lengths and bond lengths) between the cations (Fe–Al) (b, c, d, e, and f) and between the cation and anion [Fe(Al)–O] (p, q, r and s), related to the values of lattice constant; a and oxygen positional parameter, u, were calculated by eqn. (15)–(19);[25,31] values are listed in Table 2.

$$\text{Shared tetrahedral edge}: \; d_{TE} = a\sqrt{2}(2u - 1/2) \quad (15)$$

$$\text{Shared octahedral edge}: \; d_{OE} = a\sqrt{2}(1 - 2u) \quad (16)$$

$$\text{Unshared octahedral edge}: \; d_{UOE} = a\sqrt{4u^2 - 3u + 11/16} \quad (17)$$

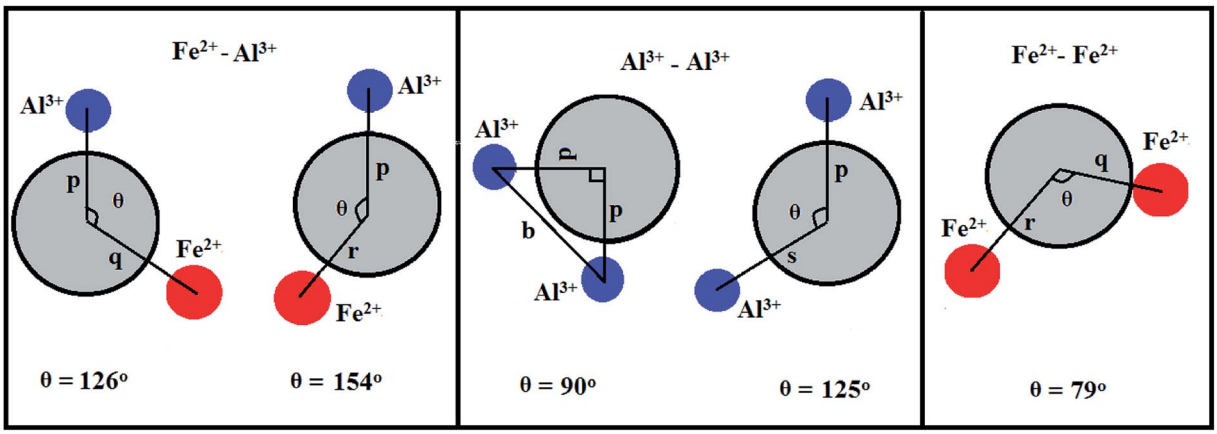

Fig. 6 Schematic representation of ion pairs in spinel ferrites with favorable distances and angles for magnetic interactions.

Table 2 Interatomic distances for $FeAl_2O_4$ spinel structure

Deposition time (min)	Oxidation time (min)	d_{TE} (Å)	d_{OE} (Å)	d_{UOE} (Å)	d_{TL} (Å)	d_{OL} (Å)
10	5	3.28232	2.49031	2.89554	2.01	1.90957
10	10	3.28232	2.48043	2.89529	2.01	1.90625
10	15	3.28232	2.48113	2.89561	2.01	1.90661
10	20	3.28232	2.49392	2.90154	2.01	1.91302

$$\text{Tetrahedral bond length}: \; d_{TL} = a\sqrt{3}(u - 1/4) \quad (18)$$

$$\text{Octahedral bond length}: \; d_{OL} = a\sqrt{3u^2 - \frac{11u}{4} + \frac{43}{64}} \quad (19)$$

It is observed from Table 2 that shared tetrahedral edge length and tetrahedral bond length are independent of oxidation time while shared octahedral edge length and bond length vary with the increase in oxidation time.

3.2. Scanning electron microscopy

Surface morphology of electrodeposited iron aluminium & iron aluminium oxide thin films are shown in Fig. 7 (a–d). Fe_3Al thin film is comprised of grains with size in the range of 0.5 μm as shown in Fig. 7(a). SEM images revealed networking, agglomeration of nano-sized particles and grain growth with the variation in oxidation time. At 10 min oxidation time morphology of iron aluminium oxide is shown in Fig. 7(b). Majority of the nanostructures have size less than 1 μm with no specific

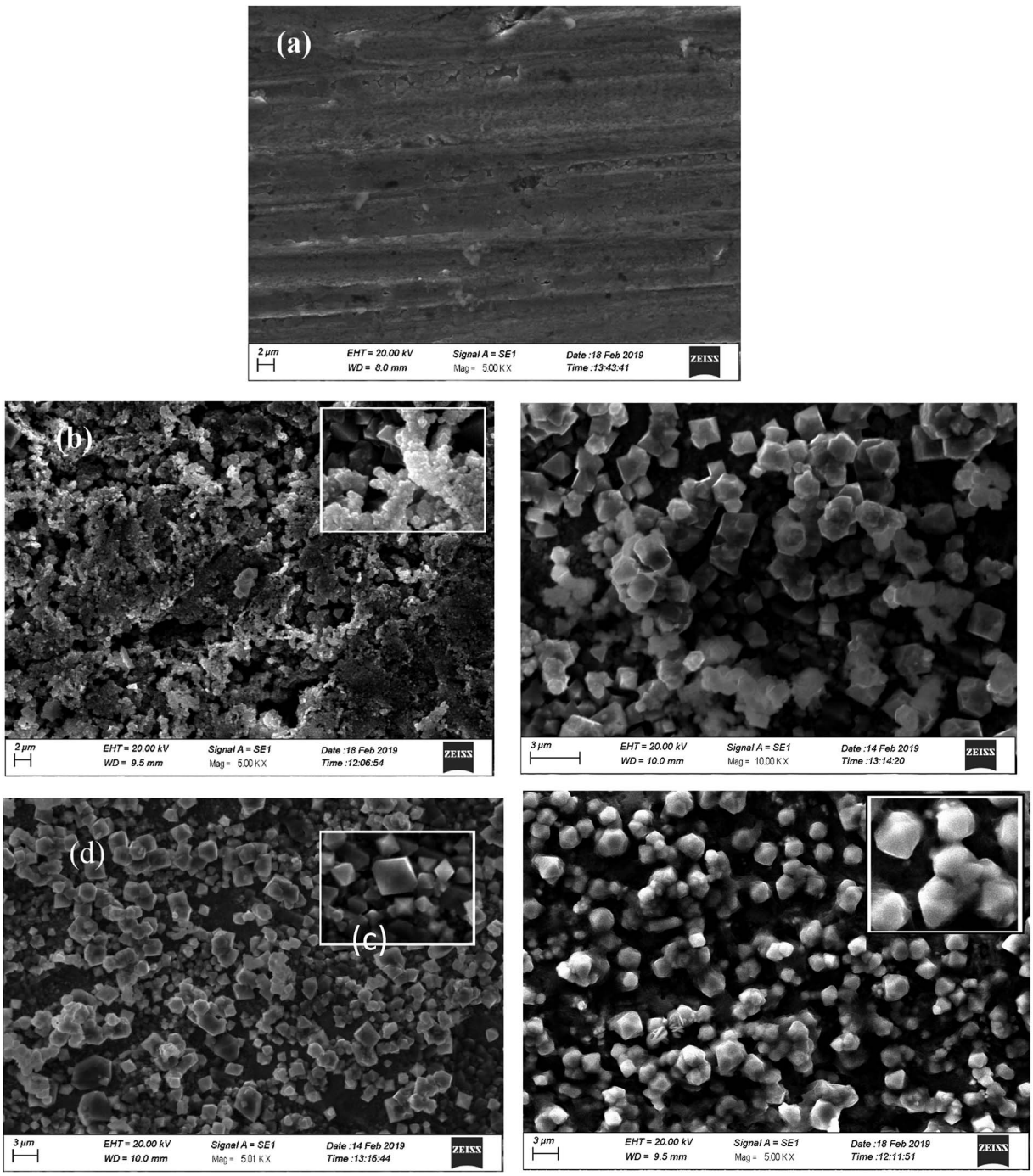

Fig. 7 SEM micrographs of (a) iron aluminium (Fe_3Al) and iron aluminium oxide thin films with (b) 10 min, (c) 15 min & (d) 20 min oxidation time.

geometry. Fig. 7(c) shows that size of these nanostructures increase with the increase in oxidation time to 15 min. Majority of these nanostructures have dodecahedral shapes while some carried octahedral shapes with size ~1.5 μm. These grains are comprised of the agglomeration of nanoparticles as can be seen in Fig. 7(c) and (d) shows fully grown ordered structures for the grains for 20 min oxidation time. Large sized grains carry dodecahedral shapes and these dodecahedrons have size of ~0.5 μm. Small sized grains carried octahedral shapes and majority of these octahedron had size less than 1 μm.

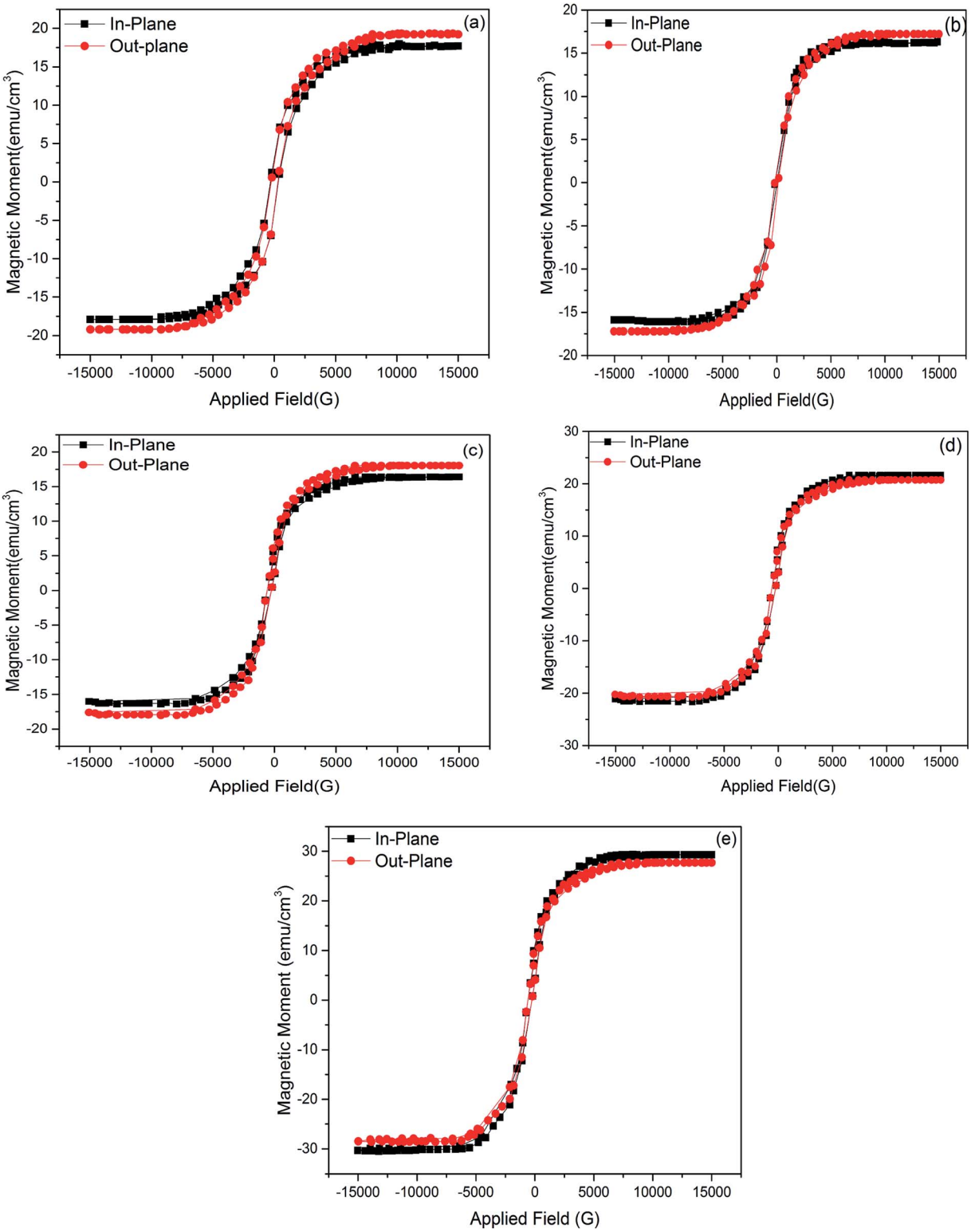

Fig. 8 *M*–*H* curves of (a) Fe_3Al and $FeAl_2O_4$ thin films with variation in oxidation time as (b) 5 min (c) 10 min, (d) 15 min and (e) 20 min.

3.3. Magnetic properties

Fig. 8(a) shows magnetic hysteresis (M–H) curves of Fe_3Al with in-plane and out of plane geometry with respect to the applied magnetic field. Fig. 8(b–e) shows M–H curves of iron aluminum oxide thin films prepared with variation in oxidation time as 5 min, 10 min, 15 min & 20 min. Ferromagnetic behavior was observed for all the thin films.

Magnetic properties in spinel structure depend on distribution of cations on tetrahedral and octahedral sites that has been discussed earlier [Tables 1 and 2]. Reported magnetic properties on iron aluminium oxide are very rare. Yaseen *et al.*[33] studied the first principle study of ferromagnetic, electronic and thermoelectric properties of iron aluminium oxide using mBJ functional approach. PBE-GGA & mBJ potentials were used to study the magnetic properties. They observed that John–Teller and exchange energies were responsible for ferromagnetism due to reduction of magnetic moment of Fe and its shifting towards non-magnetic sites. Fukushima *et al.*[6] reported ferromagnetism in iron aluminium oxide ($FeAl_2O_4$) nanoparticles under field irradiated conditions.

In electrodeposition, increase in deposition time controlled the number of metal atoms on the substrate, while oxidation time influences the oxygen positions that change octahedral site radius and octahedral lengths in the crystal structure. Variation in oxygen position (or vacancies) within the grains or across the grains may result in the exchange of electrons between Fe^{3+} and Fe^{2+} ions at octahedral sites. This hopping process induced strong ferromagnetic behavior in iron aluminium oxide thin films.[32]

Saturation magnetization (M_s), Coercivity (H_c), remanence (M_r) and exchange bias (H_{ex}) of Fe_3Al and iron aluminium oxide thin films are plotted in Fig. 9(a–d). At 0 min oxidation time, *i.e.* for intermetallic Fe_3Al thin film, saturation magnetization (M_s) was observed to be 16.81 emu cm^{-3} for in-plane and 16.95 emu cm^{-3} for out-plane geometry. The value of coercivity was observed to be 488 G for in-plane and 301.9 G for out-plane. *In situ* oxidation of Fe_3Al thin films resulted in iron aluminium oxide by anodic electrodeposition method. Increase in the value of M_s was observed with the increase of oxidation time from 5 min to 20 min. At 5 min oxidation time value of M_s was 16.1 & 17.21 emu cm^{-3} for in-plane and out-plane, respectively. Further increase in oxidation time to 10 min & 15 min resulted in very small increase in M_s from 16.4 to 16.55 emu cm^{-3} for in-plane and 17.46 to 17.6 emu cm^{-3} for out-plane. However,

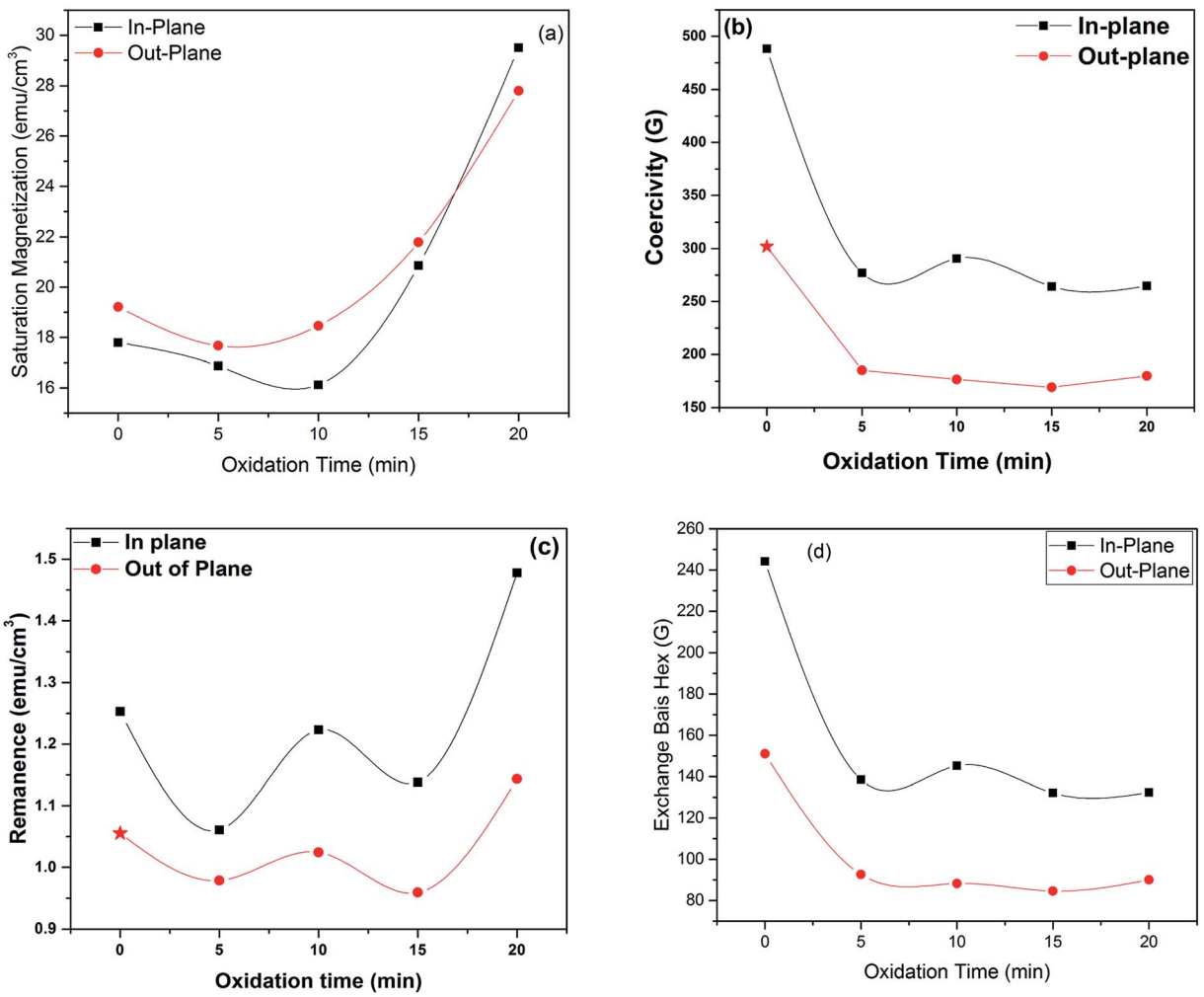

Fig. 9 Variation in (a) saturation magnetization, (b) coercivity, (c) remanance and (d) exchange bias as a function of oxidation time

remarkable increase in saturation magnetization (M_s), *i.e.* 29.5 and 27.8 emu cm^{-3} for in-plane and out-plane, respectively, was observed for 20 min oxidation time. Abrupt variation/increase in saturation magnetization (M_s) at 20 min oxidation time might have been observed due to change in shared octahedral edge length as well as octahedral bond length *i.e.* from 2.48 Å to 2.49 Å and 1.90 Å to 1.912 Å, respectively, as listed in Table 2. Further, such crystallographic changes lead to a formation of phase pure spinel $FeAl_2O_4$ [Fig. 2(e)] that is responsible for higher value of magnetization at 20 min oxidation time.

Magnetic anisotropy controls the axis of thin films along some fixed magnetic direction. Soft ferromagnetic materials have less anisotropy as compared to hard ferromagnets. Anisotropy field is the field required to saturate the magnetization of material in harder direction and it originates due to crystal structure, shape and texture of the sample. Exchange anisotropy occurs when ferromagnetic and antiferromagnetic layers are in contact and their coupling results in unidirectional anisotropy that depends on thickness between two layers and are shown in Fig. 9(d)).

Eqn (20) and (21) can be used to calculate first anisotropic constant (K_a) and exchange bais (H_{ex}).[34,35]

$$K_a = \frac{H_c M_s}{2} \tag{20}$$

$$H_{ex} = \frac{K_a}{\mu_o M_s} \tag{21}$$

It can be seen from Fig. 10(d) that exchange bias (H_{ex}) values of 242 and 143 G are observed for in-plane and out-plane geometry, respectively, for Fe_3Al thin films. Phase pure $FeAl_2O_4$ thin films, at 20 min oxidation time, resulted in low value of H_{ex}. Structural and magnetization crossover at 20 min oxidation time makes this material a promising candidate in spintronic devices as spacer layer in magnetic tunnel junctions.

Difference of saturation field dictates the easy axis of magnetization of iron aluminium oxide thin film given in eqn (22).[36]

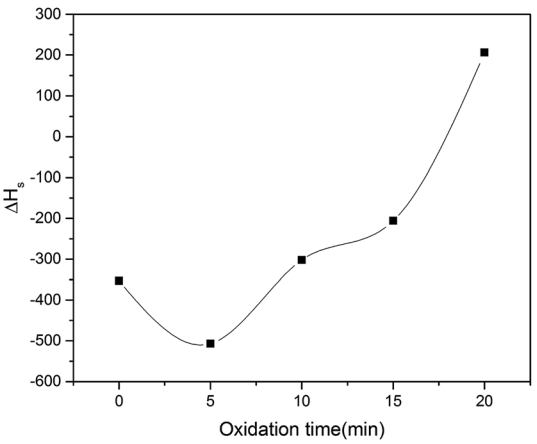

Fig. 10 Difference of saturation field of iron aluminium oxide thin film (ΔH_s)

$$\Delta H_s = H_s^{\parallel} - H_s^{\perp} \tag{22}$$

When the value of ΔH_s is positive then easy axis is parallel to the film whereas it is perpendicular when ΔH_s is negative. ΔH_s is plotted as function of oxidation time and has positive value for 20 min oxidation time and negative value for all other oxidation times as shown in Fig. 10. This change of easy axis of magnetization might be due to change of preferred orientation from (311) to (400) plane as observed in XRD patterns.

Law of approach to saturation (LAS) was used to calculate magneto crystalline anisotropy which gives useful relationship between magnetization and applied field (H) given in eqn (23).[37,38]

$$M = M_s \left[1 - \frac{a}{H} - \frac{b}{H^2}\right] + \chi H \tag{23}$$

Here M_s = saturation magnetization and χH is forced magnetization with very low value which can be ignored. "a" and "b" are constants where constant "a" is due to the presence of micro stress and "b" is crystal anisotropy and it is also associated with magneto crystalline anisotropy as given in eqn (24).[37,38]

$$b = \frac{8K_{eff}}{105{M_s}^2} \tag{24}$$

It can be seen from Table 3 that lowest value of magneto crystalline anisotropy is observed for 20 min oxidation time. Size of single domain was calculated from magneto crystalline anisotropy by using eqn (25)–(28).[37,38]

$$B = \frac{4{K_{u1}}^2}{15{M_s}^2} \tag{25}$$

$$K_{u1} = \sqrt{\frac{15|S|M_s}{4}} \tag{26}$$

$$\gamma = 4\sqrt{AK_{u1}} \tag{27}$$

$$d = \frac{9\gamma}{\mu_o {M_s}^2} \tag{28}$$

where, K_{u1} = first order anisotropy constant, S = straight-line slope, & A is the exchange stiffness coefficient with value of 4.1×10^{-7} erg cm^{-1}.

Table 3 Anisotropy constant and critical size of single domain for iron aluminium oxide thin films

Oxidation time (min)	K_{u1} (erg cm^{-3}) x 10^9	Critical size of single domain (nm)
0	1.25	273.22
5	1.30	345.24
10	0.81	257.02
15	0.18	70.23
20	0.13	54.18

4. Conclusions

A cost effective and an application oriented electrodeposition technique was used to prepare iron aluminium oxide thin films. Deposition time was kept constant, *i.e.* 10 min, for all the films, whereas, oxidation time was varied as 5 min, 10 min, 15 min & 20 min. Impure phases *i.e.* $FeAl_2O_4$ & χ-Al_2O_3 were observed at 5 min, 10 min & 15 min oxidation time. While phase pure $FeAl_2O_4$ structure was observed at 20 min oxidation time. This phase shift resulted in crossover of preferred orientation from (311) to (400). Magnetic hysteresis curves showed ferromagnetic behavior for all electrodeposited thin films. The change of easy axis of magnetization from perpendicular to parallel with high saturation magnetization ($\sim$29.5 emu cm^{-3}) and low anisotropy constant ($\sim 1.28 \times 10^8$ erg cm^{-3}) was accredited to change in preferred orientation from (311) to (400) plane at 20 min oxidation time. Such structural and magnetization crossover at 20 min oxidation time produced a potential electrodeposited material for spintronic applications such as spacer layer in magnetic tunnel junctions.

Conflicts of interest

There are no conflicts of interest to declare.

Acknowledgements

This research work is supported by Higher Education Commission (HEC), Pakistan, grant no. D/CSSP/HEC/2018-19.

References

1 S. Ramanathan, *Thin film metal-oxides*, Harvard University: Springer, New York Dordrecht Heidelberg London, 2010.
2 G. Li, Q. Dong, J. Xin, C. W. Leung, P. T. Lai, Y. W. Wong and W. P. Pong, *Microelectron. Eng.*, 2013, **110**, 192–197.
3 Z. Q. Lei, G. J. Li, W. F. Egelhoff, P. T. Lai and P. W. Pong, *IEEE Trans. Magn.*, 2011, **47**, 714–717.
4 S. Riaz, M. Azam, R. Ashraf and S. Naseem, *IEEE Trans. Magn.*, 2014, **50**, 1–4.
5 M. P. Botta, F. E. Aglietti and P. M. J. Lopez, *Mater. Chem. Phys.*, 2002, **76**, 104–109.
6 J. Fukushima, Y. Hayashi and H. Takizawa, *J. Australas. Ceram. Soc.*, 2013, **1**, 41–45.
7 R. J. Harrison, S. A. Redfern and C. S. H. O'Neill, *Am. Mineral.*, 1998, **83**, 1092–1099.
8 D. P. Dutta and G. Sharma, *Mater. Sci. Eng.*, 2011, **176**, 177–180.
9 I. Jastrzebska, J. Szczerba, P. Stoch, A. Błachowski, K. Ruebenbauer, R. Prorok and E. Snieżek, *Nukleonika*, 2015, **60**, 47–49.
10 J. Chen, L. Yu, J. Sun, Y. Li and W. Xue, *J. Eur. Ceram. Soc.*, 2011, **31**, 259–263.
11 E. Rodriguez, A. G. Castillo, J. Contreras, R. Puente-Ornelas, A. J. Aguilar-Martinez, L. Garcia and C. Gomez, *Ceram. Int.*, 2012, **38**, 6769–6775.
12 P. M. Botta, R. C. Mercader, E. F. Aglietti and J. P. Lopez, *Scr. Mater.*, 2003, **48**, 1093–1098.
13 A. Mukhopadhyay and R. I. Todd, *J. Eur. Ceram. Soc.*, 2011, **31**, 339–350.
14 G. Liu, N. Li, W. Yan, G. Tao and Y. Li, *J. Ceram. Proc. Res.*, 2012, **13**, 480–485.
15 M. Azam, A. Nairan, S. Riaz and S. Naseem, *Mater. Today: Proc.*, 2015, **2**, 5150–5154.
16 M. M. Yaqoob, S. S. Hussain, S. Riaz and S. Naseem, *Mater. Today: Proc.*, 2015, **2**, 5400–5404.
17 M. Imran, A. Raza, S. Riaz, Z. N Kayani and S. Naseem, in *World Congress on Advances in Civil*, Environmental and Materials Research (ACEM'16), 2016.
18 D. L. Hafshejani, S. Tangsir, H. Koponen, J. Riikonen, T. Karhunen, U. Tapper, P. V. Lehto, H. Moazed, A. A. Naseri, A. Hooshmand and J. Jokiniemi, *Powder Technol.*, 2016, **298**, 42–49.
19 T. Blank, B. Leyrer, T. Maurer, M. Meisser, M. Bruns, M. Weber, in *Proceedings of the 5th Electronics System-Integration Technology Conference*, ESTC, 2014, 1–6.
20 J. T. C. Low, A. G. R Wills and C. F. Walsh, *Surf. Coat. Technol.*, 2006, **201**, 371–383.
21 D. Iselt, A. Funk, L. Schultz and H. Schlorb, *ECS Electrochem. Lett.*, 2013, **3**, D13–D15.
22 F. M. Ashby, J. P. Ferreira and L. D. Schodek, *Nanomaterials, Nanotechnologies and Design, 1st Edition*, Elsevier, 2009, p. 262.
23 I. Zhitomirsky, *JOM*, 2000, **52**, 45774–24607.
24 M. Paunovic, *Mod. Electroplat.*, **1**, 433–446.
25 B. D. Cullity, *Elements of X-ray Diffraction*, Addison-Wesley Publishing Company, Inc., Boston, 1956.
26 S. S. Shojaeenezhad, M. Farbod and I. Kazeminezhad, *Journal of Science: Advanced Materials and Devices*, 2017, **2**, 470–475.
27 M. A. Gabal, M. R. El-Shishtawy and M. Y. Al Angari, *J. Magn. Magn. Mater.*, 2012, **324**, 2258–2264.
28 S. Rehman, S. Riaz, S. S. Hussain, Y. B. Xu, S. Naseem, in *World Congress on Advances in Civil*, Environmental and Materials Research (ACEM'16), 2016.
29 K. Kugimiya and H. Steinfink, *Inorg. Chem.*, 1968, **7**, 1762–1770.
30 R. Sharma and S. Singhal, *Phy. B: Cond. Mat.Phys. Rev. B: Condens. Matter Mater. Phys.*, 2013, **414**, 83–90.
31 S. M. Attia, *Egypt J Solid*, 2006, **29**, 329–340.
32 F. Mukhtar, Z. N. Kayani, S. Riaz and S. Naseem, *Ceram. Int.*, 2018, **44**, 9550–9560.
33 M. Yaseen, Q. Mahmood, S. M. Ramay, I. Ali, Y. M. Naz and A. Mahmood, *J. Supercond. Novel Magn.*, 2018, **31**, 1435–1441.
34 M. Birkholz, *Thin film analysis by X-ray scattering*, John-Wiley and Sons., 2006.
35 J. M. D. Coey, *Magnetism and magnetic materials*, Cambridge University Press., 2010.
36 Lecture Notes in Physics. in *Spin Electronics*, ed. M. J. Thornton and M. Ziese, vol. 569, 2001.
37 B. D. Cullity, C. D. Graham, *Introduction to Magnetic Materials*, John-Wiley and Sons, 1972.
38 Y. Peng, X. Wu, Z. Chen, W. Liu, F. Wang, X. Wang and V. G. Harris, *J. Alloys Compd.*, 2015, **630**, 48–53.

